RANDOM DIODE ARRAYS AND MESOSCALE PHYSICS OF LARGE-AREA SEMICONDUCTOR DEVICES

V. G. Karpov,* A. D. Compaan, and Diana Shvydka
Department of Physics and Astronomy, University of Toledo, Toledo, OH 43606
(Dated: July 2, 2003)

Large-area, thin-film semiconductor devices often exhibit strong fluctuations in electronic properties on a mesoscale level that originate from relatively weak microscopic fluctuations in material structure such as grain size, chemical composition, and film thickness. Amplification comes from the fact that electronic transport through potential barriers is exponentially sensitive to the local parameter fluctuations. These effects create new phenomena and establish the physics of large-area, thin-film devices as a distinctive field of its own, quite different from that of microelectronics. We show that (i) large-area semiconductor thin-film devices are intrinsically nonuniform in the lateral directions, (ii) the nonuniformity can span length scales from millimeters to meters depending on external drivers such as light intensity and bias, and (iii) this nonuniformity significantly impacts the performance and stability of, *e.g.*, photovoltaics, liquid crystal displays, and light emitting arrays. From the theoretical standpoint our consideration introduces a new class of disordered systems, which are random diode arrays. We propose a theory describing one class of such arrays and derive a figure of merit that characterizes the significance of nonuniformity effects. Our understanding suggests some methods for blocking the effects of nonuniformities.

PACS numbers: 73.50, 73.61.J, 73.61.G, 78.66.H, 85.30

I. INTRODUCTION

Large-area semiconductor thin films play a key role in such rapidly growing fields as terrestrial photovoltaics (PV), flat-panel emissive displays, and liquid-crystal displays (LCD). With active-area requirements of about one square meter for PV and 0.1-1m^2 for displays, the films cannot be deposited epitaxially (crystalline) but are either polycrystalline or amorphous. In this paper we show how the intrinsic polycrystalline or amorphous character of the films together with electronic transport that is exponentially sensitive to fluctuations in local material parameters, leads to strong fluctuations in electronic properties. Controlling or blocking the effects of these fluctuations can be the key not only to the fabrication of a high performance device, but is often critically important to reducing the performance deterioration over time.

We believe that the nonuniformity effects create new phenomena and establish the physics of large area thin-film devices as a distinctive field of its own, quite different from that of microelectronics. This paper is aimed at presenting the above-defined field to a broader audience. It generalizes recent data for major semiconductors that we have managed to relate to each other in the framework of a unique approach. In our work we derive a fundamental length scale that discriminates between the cases of small and large-area devices, and beyond which a new physics emerges. Large-area electronics is shown to be intrinsically nonuniform, which significantly affects the device physics. We feel that enhanced understanding of the effects of nonuniformities will help to improve thin-film device performance and stability in many applications. From the theoretical perspective, our consideration introduces a new type of disordered systems, random diode arrays), which exhibit nontrivial behavior, are practically important and remain poorly understood.

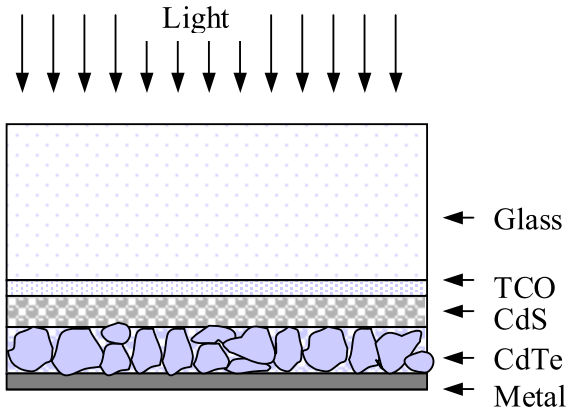

FIG. 1: CdTe/CdS solar cell structure (not to scale). Polycrystalline structure of CdTe film is schematically shown.

For illustration, we shall focus our discussion on a simple PV cell, although our argument is extendable to other devices. The essential cell structure (Fig.1) is a thin-film p-n junction a couple of microns thick (for example, CdTe/CdS) sandwiched between two electrodes, one of which is transparent to light (typically, a transparent conductive oxide, TCO). The grains have comparable or somewhat smaller lateral dimensions, 0.1 - 1 μm. Both one-dimensional, 1D (stripe cell) and 2D (dot cell) devices are of interest, with characteristic linear dimensions d $\sim$2 - 10 mm. The PV cell parameters and their order-of-magnitude estimates under a light intensity of one sun (100 mW/cm^2) are: open-circuit voltage, $V_{oc}\sim$1V, and short-circuit current density, $j_{sc}\sim 10^{-2}$

A/cm^2. The transparent electrode sheet resistance is typically $\rho \sim 10\Omega/\Box$, while the other electrode resistance is negligibly small.

Our emphasis in this work is on the lateral device nonuniformities. These originate from relatively weak local fluctuations in the material parameters such as grain size, chemical composition and film thickness, but they translate into strong fluctuations in the electronic properties. The amplification comes from the fact that electronic transport through the potential barriers is exponentially sensitive to the local parameter fluctuations in both the temperature-activated and tunnelling modes. Indeed, for a barrier of height V_B and width a, the corresponding barrier transmission probabilities, $\exp\left(-V_B/kT\right)$ and $\exp\left(-2a\sqrt{2mV_B}/\hbar\right)$ typically have exponents much greater than one. Hence, their relatively small variations cause significant effects. Here k is Boltzmann's constant, T is the temperature, m is the electron mass, and $\hbar$ is Planck's constant. The barriers in PV cells are associated with the device junctions (p-n, semiconductor/TCO, and semiconductor/metal) and grain boundaries. The current density vs. bias voltage V is specified in the ideal photo-diode model as[1]

$$j = j_T\left[\exp\left(\frac{eV}{kT}\right)-1\right]-j_{sc}, \qquad (1)$$
$$V_{oc} = \frac{kT}{e}\ln\left(\frac{j_{sc}+j_T}{j_T}\right).$$

The short circuit current j_{sc} is typically linear and the open-circuit voltage V_{oc} is logarithmic in the light intensity. Also, it is typical that the thermal current component, j_T is much less than the photocurrent component j_{sc} for all practically interesting light intensities.

Eq. (1) can be equally represented in the form

$$j = j_0\left\{\exp\left[\frac{e(V-V_{oc})}{kT}\right]-1\right\}, \quad j_0 \equiv j_{cs}+j_T, \quad (2)$$

which shows that V_{oc} is intimately related to the junction barrier height. Its fluctuations become exponentially significant if they exceed kT. The available data below (see Sec. II) show that the latter inequality does obey.

We recall that the thermal current j_T is significantly determined by the system potential barriers[1] and thus is exponentially sensitive to the material parameter fluctuations. To the contrary, j_{sc} is relatively uniform because the p-n junction electric field is everywhere strong enough to effectively separate the light generated electrons and holes determining j_{sc} (this is also reflected in the device high quantum efficiency, typically $\sim 0.6-0.9$).

In the terms of the parameters in Eq. (2), the latter consideration means that j_0 is relatively insensitive to the material fluctuations, while V_{oc} fluctuates considerably and is intimately related to fluctuations in the system potential barriers. Because V_{oc} has exponentially strong effect on the current [Eq. (2)], it is considered the main fluctuating parameter in the system.

Experimentally, lateral nonuniformities are often masked by low resistance contacts that level out the electric potential variations across the cell through lateral current flow in the contacts. As explained in detail below, lateral currents cause resistive losses and nonuniform device degradation. Therefore, although low resistance contacts make the nonuniformities less visible, they contribute detrimental side effects. To circumvent this masking effect, the nonuniformities are best studied either in unfinished devices (without metal contact), in devices with intentionally high resistance contacts, or in processes that are relatively independent of metal contacts, such as charge carrier recombination or collection.

Lateral nonuniformities can also show up in parameter variations among nominally identical devices. For example, it is typical to observe noticeable (∼10%) experimental differences between cells ∼1 cm apart on the same substrate, as is illustrated in Fig. 2. This observation is not often addressed in academic reports and remains mostly folklore. However, the issue of such variations becomes commercially important in large-scale production[2].

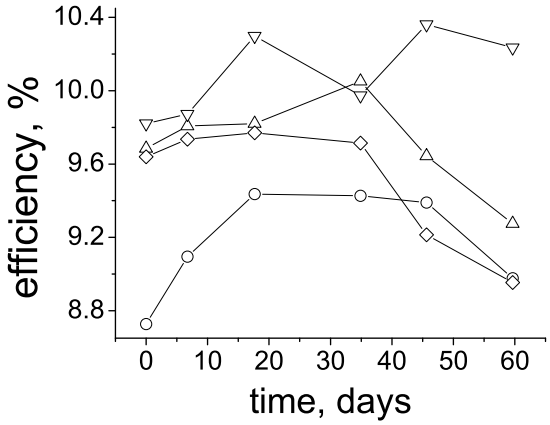

FIG. 2: An example of differences in initial efficiencies and degradations of four nominally identical CdTe/CdS solar cells on the same substrate.

Our paper is organized as follows. In Sec. II we find it appropriate to give a brief review of the relevant data on major PV material nonuniformity effects (which, to our knowledge, is the first such review ever published). Sec. III introduces new theoretical concepts of random diode arrays and lateral screening in a device underlying the physics of laterally nonuniform devices. A theory of random diode systems has never been fully developed and remains in its infancy. We employ a semi-quantitative approach aimed at understanding the basic phenomena is random diode arrays. In Sec. IV we analyze the main mesoscale effects that show up in macroscopic voltage, current, their fluctuations, and the phenomenon of nonuniform degradation. In Sec. V we describe our attempts of developing more quantitative theory of random

diode arrays. Based on our understanding, in Sec. VI we suggest some practical ways of blocking the nonuniformity effects. Sec. VII contains conclusions.

II. SURVEY OF MESOSCALE NONUNIFORMITY OBSERVATIONS

Published reports on nonuniformities in thin-film devices are rare, and to our knowledge have never been reviewed. Yet, the available data show significant V_{oc} and electric current variations among nominally identical devices in noncrystalline thin-film structures. They typically represent the results of device mapping using either direct electrical measurements or more sophisticated techniques, such as optical-beam-induced current (OBIC), electron-beam-induced current (EBIC), and scanning-tunnelling microscopy (STM). Below we briefly review the results for several major materials.

For local microscopic V_{oc} measurements (also termed surface photovoltage for the case of devices without a metal contact), drastic lateral variations ranging from 0.2 to 0.7 V between different grains were detected by STM for a Cu(In,Ga)Se_2 polycrystalline PV device.[3] These fluctuations were attributed to observed local variations in the film chemical composition. For similar devices, OBIC revealed microregions of reduced photovoltaic efficiency.[4] The latter do not correlate with visible irregularities and were described as low V_{oc} regions. In large-area $CuInSe_2$ PV modules, long length scale (millimeter to centimeter) inhomogeneities were found to correlate with lower device performance.[5] In particular, mapping of V_{oc} and other parameters revealed nonuniformities in average modules which were not present in the best modules. They were attributed to macroscopic imperfections such as defects in the glass substrate or contaminants in the film. Considerable variations between nominally identical CIGS devices were found.[6]

For CdS/CdTe polycrystalline PV cells, OBIC[7] and EBIC[8–10] showed strong inhomogeneities dependent on postdeposition treatments with length scales ranging from microns to millimeters. For CdTe PV modules, OBIC indicated considerable inter– and intra– cell variations,[11] with the exception of some cases where cells were laterally quite uniform.[12] Time-resolved photoluminescence in CdS/CdTe solar cells revealed variations in recombination lifetime, by a factor of two to three across one cm distances.[13] Photoluminescence mapping[14]also showed considerable nonuniformities on a large ($\sim$ 1 mm) scale whose topology depends on the excitation laser-beam power. Scanning ballistic electron emission spectroscopy (a variation on STM) revealed the barrier height dispersion of approximately 0.1 eV across an area of 10 μm^2 in a crystalline CdTe/metal junction.[15,16] For the polycrystalline CdTe/CdS cell our STM mapping leads to results[17] similar to those for CIGS in Ref. 15. Mapping of a polycrystalline CdTe cell fabricated with a high resistance contact[18] showed $\sim$ 0.2 V electric potential variations over a 1 cm length scale and lateral nonuniformities in the temperature field distribution under 1 sun irradiation. A typical 10×10 cm^2 voltage map in Fig. 3 shows both the true shunt feature and other lateral nonuniformities. Nonuniform degradation of short-circuit current in CdTe cells was noticed in Refs. 19 and 20. Strong effects of nonuniformity on commercial CdTe photovoltaics were discussed in Ref. 21.

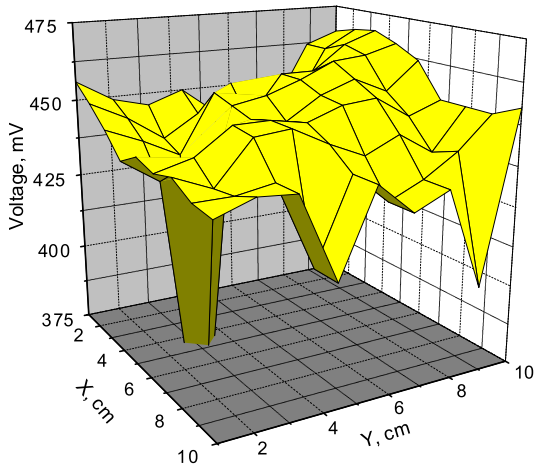

FIG. 3: Open circuit electric potential variations of CdS/CdTe vapor transfer deposited sample with intentionally high resistive back contact (10 nm Chrome) under low light of 0.01 sun. The main feature at X = 4 cm, Y = 3 cm represents a true shunt with voltage drop down to 0.05 V (cut off in the diagram).

For the case of a-Si:H, changes in photoinduced degradation, defect density and PV parameters were found to depend on nano- and longer length scales of structural inhomogeneity.[1,22,23] Lateral nonuniformities in V_{oc}, j_0 and other parameters were identified in micro-, multi-, and polycrystalline silicon.[24–30] In particular, it was shown[31–33] that forward current through a multicrystalline cell does not flow homogeneously and is dominated by local sites of diode nature different from the standard ohmic shunts.

Schottky diodes have proven to be inhomogeneous even when based on crystalline semiconductors.[34–38] This implies again that barrier-controlled electron transport is exponentially sensitive to local fluctuations in material parameters. Existing theories attribute such fluctuations either to electric charge density (which affects the barrier height)[39] or to fluctuations in defect concentration that affect the barrier tunnelling transparency.[40] Highly nonuniform charge flow induced by ionized defects within a crystalline semiconductor junction is evidenced also in the pitted submicron morphology ob-

tained by photoetching.[41] Due to nonuniformities, an effective area involved in the current transport becomes significantly lower than the geometric area of the metal semiconductor/interface.[42]

Technologically, nonuniformity length scales ranging from microns to tens of centimeters can originate from different process steps. For example, polycrystalline film growth kinetics is generically nonuniform. The dispersion in grain sizes translates into variations in the curvature-dependent impurity gas pressure at grain boundaries which affects their doping levels and leads to micron-scale nonuniformities. Submicron nonuniformities originate then from the intragrain fluctuations in doping and stoichiometry.[43] Variations with length scales longer than the grain size are likely to be due to the postdeposition grain coarsening treatment. Wet treatments and droplet dry-up can lead to nonuniformities with 100 μm to 1 cm scales governed by surface tension. Module-size length scales originate from nonuniformities in the deposition device. During the complete fabrication cycle, from deposition to final product, nonuniformities of different nature and length scales superimpose. We emphasize that the processes involved are intrinsically nonuniform and thus lateral inhomogeneities of the material parameters in large-area, thin-film devices are unavoidable.

III. UNDERSTANDING LATERALLY NONUNIFORM DEVICES

The explanation of the lateral fluctuations under consideration lies in the device diode nature and in the presence of the resistive electrode. This is reflected in the equivalent circuit of random microdiodes in Fig.4 that we call a random diode array. In accordance with the above discussion, each microdiode in the array is described by the voltage-current characteristics of Eq. (2) where V_{oc} is a random parameter and fluctuations in j_0 are neglected. The microdiode size is of the order of the nonuniformity length scale l.

In general, the effects of lateral micrononuniformities depend on the relationship between the nonuniformity length scale l and the screening length

$$L(u) = \sqrt{|u|/\rho j_0}, \tag{3}$$

where $u(< 0)$ is the local fluctuation of electric potential. The physical meaning of L is that the fluctuation in electric potential is balanced by the potential drop $j_0 L^2 \rho$ across the resistive electrode of linear dimension L. The latter applies to both the cases of one-dimensional (D=1) and two-dimensional (D=2) cell (see Sec. I). For D=1, $L\rho$ and $j_0 L$ represent the resistance and current, and ρ is understood as the resistance per unit length. For D=2, the resistance is represented by the sheet resistance ρ and the current is $j_0 L^2$. The maximum screening length $L_{\max}$ corresponds to a dead shunt ($u = V_{oc}$). The minimum screening length L_0 is defined by Eq. (3) with $u = kT/e$.

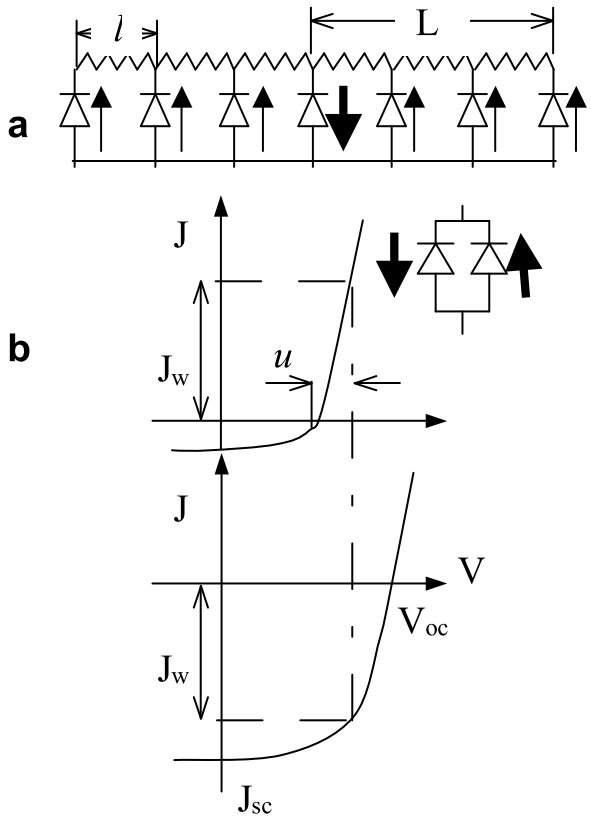

FIG. 4: **a**, equivalent circuit of random microdiodes representing laterally nonuniform photovoltaic devices. Fat arrow shows shunting current (J_w) through the weak diode, with polarity opposite to that of the photogenerated currents supplied by the majority of diodes. L is the screening length. **b**, The equivalent two-diode circuit (inset) and J/V characteristics of the weak diode (shunting the current J_w) and its more robust neighborhood (supplying the current $-J_w$). Because of the difference in the diode V_{oc}'s the weak diode finds itself under forward bias u.

Generally, the length L varies over a wide range depending on the sheet resistance and photocurrent. For example, given the device characteristic parameters in Sec. I, the screening length $L_0 \sim 1$ mm under 1 sun illumination. The typical ambient room light (and corresponding current j_0) is roughly by four orders of magnitude lower; hence, $L_0 \sim 10$ cm and $L_{\max}$ can be as large as 1 m. Note however that both lengths can be shorten significantly by using high resistance electrode (increasing ρ).[45]

The screening length in Eq. (3) was for the first time derived in Ref. 44 to describe shunt and local bias screening. The minimum screening length L_0 was introduced much earlier[46] in connection with photoeffects in nonuniformly irradiated p-n junctions. Because in Ref. 46 L_0 appeared in a formal way, we find it appropriate to give here its intuitive derivation similar to that of Eq. (3) above. We start with recalling that [in accordance with Eq. (2)] a potential $\delta V + V_{oc}$ slightly different from the

open circuit voltage, $|\delta V| \ll V_{oc}$, forces the diode current $\delta V/R_{oc}$ where $R_{oc} = kT/ej_0$ is the open circuit resistance. Similar to the derivation of Eq. (3), δV is balanced by the potential drop across the resistive electrode of linear dimension L_0, i. e. $\delta V = j\rho L_0^2\rho$. Substituting here $j = \delta V/R_{oc}$ gives

$$L_0 = \sqrt{\frac{kT}{ej_0\rho}} \tag{4}$$

for both the cases of D=1 and D=2. Note the main cause of the difference between L and L_0: in the latter case the current is linear in a small deviation of the electric potential from V_{oc}. To the contrary, in the case of strong local perturbations, it was independent of the potential and close to its saturated value j_0.

Eqs. (3), (4) describe screening of a point perturbation. For a system of multiple random diodes, we first point out a trivial case when the screening length is much shorter than the nonuniformity length scale ($l >> L$) and the neighboring units are electrically insulated. The observed quantities then correspond to a locally tested microdiode. Note that because the regions at distances larger than L make no contribution, L sets the upper limit to the size of an efficient cell.

Given the range of L from ~ 1 mm to ~ 1 m and the much shorter fluctuation length scale l (~ 1 μm), the opposite limiting case of strongly interacting microdiodes, $l << L$ is practically important. This case is illustrated in Fig.4 where two diodes in parallel mimic a weak element (low V_{oc}) and its more robust neighbors (high V_{oc}). The former finds itself under forward bias u and correspondingly strong positive current [cf. Eq. (2)]

$$j_w \approx j_0 \exp\left(|eu|/kT\right) \tag{5}$$

supplied by the diodes in the surrounding region within the screening length. A weak microdiode robs currents from a large number

$$N_L = j_w/j_0 = (L/l)^D >> 1 \tag{6}$$

of its more robust neighbors, thereby significantly lowering the device efficiency. Such non-ohmic shunting does not affect the performance in reverse bias, as do the standard ohmic shunts.

By expressing the ratio j_w/j_0 from Eqs. (5) and (6) one can define the characteristic crossover potential

$$u_c = \frac{DkT}{e} \ln\left(\frac{L}{l}\right), \tag{7}$$

between the regimes of weak and strong local perturbations.[47] Its physical meaning is that a weak bare perturbation $u < u_c$ is completely levelled out (down to the thermal potential kT/e) by large screening photocurrents in the range L. To the contrary, because there is not enough photocurrent, a strong bare perturbation $u > u_c$, cannot be screened completely; its screened value $u - u_c$ causes noticeable lateral potential variation.

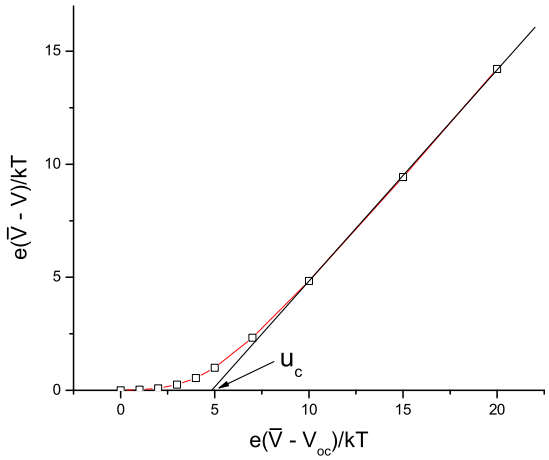

FIG. 5: An example of numerically simulated voltage (V) across a 'foreign' diode of open-circuit voltage V_{oc} imbedded into a large system of equivalent diodes of the open-circuit voltage $\overline{V}$ each. Straight line shows the approximation in Eq. (8).

In particular, a single weak diode whose V_{oc} is lower than the surrounding media potential ($\overline{V}$) by less than u_c, finds itself under potential $V = \overline{V}$. However, a weaker diode of $V_{oc} < \overline{V} - u_c$ will be under potential $V < \overline{V}$, that is

$$V = \begin{cases} \overline{V} & \text{for} \quad V_{oc} > \overline{V} - u_c \\ V_{oc} + u_c & \text{otherwise} \end{cases} \tag{8}$$

The approximation of Eq. (8) is illustrated in Fig. 5.

One other reading of Eq. (8) is that there exists a parameter

$$\xi_L \equiv \left(\frac{l}{L}\right)^D \exp\left[\frac{e(\overline{V} - V_{oc})}{kT}\right], \tag{9}$$

such that the weak diode effects are relatively small when $\xi_L \ll 1$ and are significant when $\xi_L \gg 1$.

Eq. (6) needs an obvious correction if there are several equally weak diodes in the region of the length L. More specifically, we note that, side by side with the above-defined L, there is another characteristic length describing the system of random diodes. This is the correlation radius R. Its standard physical meaning is that the system is macroscopically uniform on length scales longer than R. A simple nonrestrictive example is a bimodal V_{oc} distribution representing identical weak (low V_{oc}) diodes imbedded in the uniform matrix of more robust units. For the case of bimodal distribution, R is the average distance between the nearest weak diodes. To estimate R for a continuous V_{oc} distribution we note that, in accordance with Eq. (2), the number of significantly different microdiodes in the system is $e\Delta/kT$, where Δ is the characteristic width of the distribution. Because

each of the diodes has the linear dimension l, we find $R = l\,(e\Delta/kT)^{1/D}$. The inequality $R << L$ is consistent with the available data in Sec. II. Replacing $L \to R$ and combining Eq. (6) with Eq. (5) gives the maximum local bias (across the weakest microdiodes) and the corresponding screening length in the system,

$$u_w = D\frac{kT}{e}\ln\left(\frac{R}{l}\right), \quad L_w = L_0\sqrt{D\ln\left(\frac{R}{l}\right)}. \qquad (10)$$

Thus, a weak diode is biased significantly, $u_w > kT/e$ and its screening length is macroscopically large, $L_w >> l$.

Spacial fluctuations in the weak diode concentration cause the electric potential and current fluctuations of the length scales of the order of L. To estimate these effects in a system of $N = (L/R)^D \gg 1$ weak diodes we note that the relative fluctuation in their number is $\delta N/N \sim 1/\sqrt{N} \sim (R/L)^{D/2}$. Taking into account that each weak diode consumes exponentially strong relative current $\exp[e(\overline{V} - V_{oc})/kT]$, one can define a disorder parameter

$$\xi_R \equiv \left(\frac{R}{L}\right)^D \exp\left[2\frac{e(\overline{V} - V_{oc})}{kT}\right], \qquad (11)$$

such that the disorder effects are small when $\xi_R \ll 1$ and are significant when $\xi_R \gg 1$. ξ_R describes the relative dispersion in the weak diode currents. In deriving Eq. (11) all the weak diodes were, for simplicity, assumed to have the same V_{oc} (lower than the average voltage $\overline{V}$). In Sec. V the parameter $\xi \approx \xi_R$ is derived in a more rigorous way for a general case where weak diodes can have different V_{oc}'s [see Eqs. (34) and (36)] and is shown to be a figure of merit for the weak diode effects.

In the above we have been assuming implicitly the V_{oc} distribution to have an effective cut-off width Δ. A conceivable alternative model assumes a probability distribution of open circuit voltages, $g(V_{oc})$, having a long exponentially decaying tail. In the latter case the situation is considerably different from that described by Eq. (10), that is, very rare but extremely weak diodes will rob the most current. The correlation length then becomes exponentially large and is determined by the optimum fluctuation that finds the weakest diode with finite probability. This occurs when the product $g\,(V_{oc})\exp\,(-eV_{oc}/kT)$ is a maximum. Assuming, for example, the Gaussian distribution with the dispersion Δ^2 this model yields the correlation radius

$$R = l\exp\left[\left(\Delta e/kT\sqrt{D}\right)^2\right], \qquad (12)$$

which at low temperatures can exceed both the screening radius and the linear dimensions of the device.

IV. MESOSCALE EFFECTS OF MICRONONUNIFORMITIES

Micrononuniformities have significant effects on the macroscopic voltage and current as well as the device degradation as discussed below. They are determined by the length scales of the order of the above introduced screening length, $L \sim$ 1mm to 1 m, which may be comparable to the devices size; we call these effects mesoscale.

A. Macroscopic voltage

The random diode array in Fig.4 can be simulated by numerically solving the corresponding Kirchhoff's equations for a given random input parameter distribution. In Fig.6 the calculated output parameter distributions show indeed weak microdiodes whose V_{oc}s are lower than the local electric potential V; they force strong positive currents. Under open circuit, they balance small negative currents flowing through the majority of microdiodes (with $V < V_{oc}$). The electric potential V varies much less than V_{oc} because its fluctuations are averaged out over $N >> 1$ mutually interacting microdiodes.

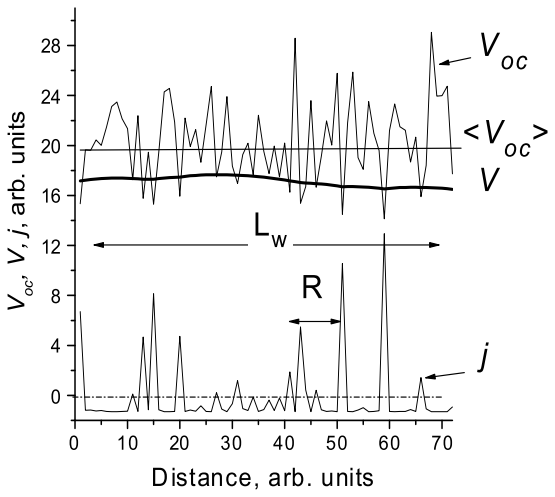

FIG. 6: Simulated open-circuit voltage (V_{oc}), electric potential (V), and transverse electric current (j) distributions in an open-circuit system of random diodes. Rare strong positive currents correspond to weak diodes balancing the majority of robust diode currents, which are negative. Note that the robust diode negative currents are practically the same as they would be under short-circuit conditions. The correlation radius (R) and the weak diode screening radius (L_w) are also shown.

For the case of $L >> R$ it is possible to describe the macroscopic electric potential analytically. Consider $N >> 1$ diodes occupying a volume of linear dimension $x << L$, but still macroscopically uniform in the sense $x >> R$. Because $x << L$, the resistive potential drop across the domain is relatively small and the diodes are under almost the same potential $\overline{V}$. The latter can be found by setting to zero the sum of $N = (x/l)^D$ random

currents [each given by Eq. (2) with $V = \overline{V}$],

$$\overline{V} = -\frac{kT}{e} \ln \left\langle \exp\left(-\frac{eV_{oc}}{kT}\right)\right\rangle_N . \qquad (13)$$

Since $N >> 1$, the above average is close to the true arithmetic average, which can be calculated based on the statistical distribution for V_{oc}. Following Eq. (13), the characteristic potential fluctuation is

$$\delta V = \frac{kT}{e\sqrt{N_L}} \frac{\delta\left[\exp\left(-eV_{oc}/kT\right)\right]}{\left\langle \exp\left(-eV_{oc}/kT\right)\right\rangle_{N_L}}, \qquad (14)$$

where we have taken into account that independent fluctuations have a linear dimension $x = L_w$. Eqs. (13) and (14) agree well with the results of numerical simulations. For example, the uniform V_{oc} distribution with the lower bound $V_{oc,\min}$ and width $\Delta = V_{oc,\max} - V_{oc,\min}$ is characterized by

$$\overline{V} = \min\left[V_{oc,\min} + (DkT/e)\ln\left(R/l\right), V_{oc,\max}\right] \qquad (15)$$

and

$$\delta V = \Delta\left(l^2/L_w R\right)^{D/2}. \qquad (16)$$

Because for the opposite case of $R \gg L$ the above consideration fails, we develop the effective medium approach. Along the standard lines, the effective medium sought is an imaginary homogeneous system whose parameters coincide with the average parameters of the non-homogeneous system under consideration. Consider a single foreign diode embedded into a uniform effective medium consisting of identical diodes of the open circuit voltage $\overline{V}$. In our approximation $\overline{V}$ is the only effective medium parameter. The voltage drop V across the foreign diode is a function of its bare open circuit voltage V_{oc} and $\overline{V}$,

$$V = V(V_{oc}, \overline{V}). \qquad (17)$$

In the original nonuniform system we apply Eq. (17) to an arbitrary diode and approximate its surroundings by the effective uniform medium. Selfconsistency dictates that, as averaged over all such diodes, the voltage V in Eq. (17) is equal to the effective medium open circuit voltage,

$$\overline{V} = \int dV_{oc} g(V_{oc}) V(V_{oc}, \overline{V}), \qquad (18)$$

where $g(V_{oc})$ is the probability distribution of microdiode open circuit voltages.

To describe the dependence in Eq. (17) we employ the approximation in Eq. (8). Using for simplicity the uniform distribution $g = 1/(V_{oc,\max} - V_{oc,\min})$ Eqs. (18), (8) yield

$$\overline{V} = \min\left[V_{oc,\min} + \frac{DkT}{e}\ln\left(\frac{L}{l}\right), V_{oc,\max}\right]. \qquad (19)$$

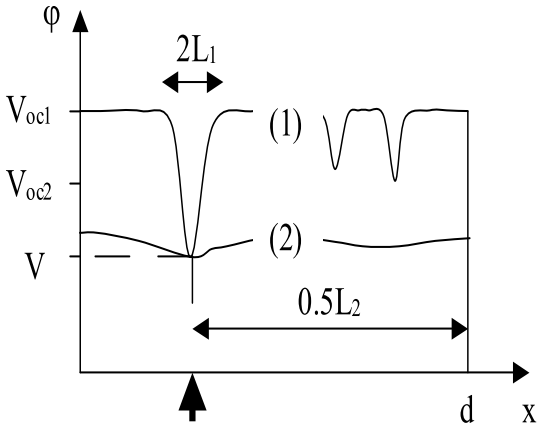

FIG. 7: Electric potential distribution along the resistive electrode, which is the TCO for the standard cells and 5 nm Cr contact for the high resistive electrode cells. The measuring probe (fat arrow) applies voltage bias V. The cases of (1) small and (2) large L/l are shown. For illustration purposes, the cell is uniform to the left of the probe and nonuniform to the right of it. In the case (1) the nonuniformities are screened ($L_1 \ll d$) and do not affect the current collection, as opposed to the case (2) where they compete for the current with the probe ($L_2 \gg d$).

As applied to the former case of $R \gg L$, the result in Eq. (19) changes by R replacing L under the logarithm, which makes it identical to that in Eq. (15) and thus adds credibility to the present effective medium approach.

In general, since the balance of currents (rather than V_{oc}) determines the average macroscopic potential, the weak diode contribution is exponentially significant; in particular, a strong inequality $\overline{V} > \langle V_{oc}\rangle$ takes place, as is also illustrated in Fig.6. In other words, under open-circuit conditions, the recombination of photogenerated electrons occurs mostly through weak diodes, as opposed to the ideal system where the recombination is spatially uniform. The degree of nonuniformity in local V_{oc} needed to cause the above qualitative difference is as low as several kT/e, well within the observed range of the V_{oc} fluctuation data. (See Section II.)

B. Macroscopic current

Under working conditions, the current is partially consumed in the external circuit. Its flow corresponds to the electric field E_j, which is a maximum at the proximity of a contact (probe) and vanishes at some point where the current is zero (for example, $E_j = 0$ at the cell edges; see Fig. 7). At a point with coordinate $x \le d$ one can estimate $E_j(x) \sim |j|\,\rho d\,(1 - x/d)$ for both the cases of D=1 and D=2, where j is the measured current density. In regions where the field is weak the conditions are

close to that of open circuit. In such a quasi-open-circuit region weak microdiodes are most detrimental and may rob a significant amount of current. The size of that region is determined by the condition $E_j(x) = E_w$, where $E_w \sim u_w/L_w \sim \sqrt{u_w |j| \rho}$ is the weak microdiode field. Because the latter decreases with j slower than $E_j \propto j$, it is clear that the size of the quasi-open-circuit region increases and weak microdiodes become more important at low currents. More specifically, the dimension of the region is $\Delta x = L_w$. As seen from the definition of L_w in Eq. (10), Δx and the current loss decrease with $|j(V)|$ and are almost minimum under short-circuit conditions where the current is close to its maximum value. Forward bias decreases $|j(V)|$, thus increasing L_w and the current loss. As a result the curvature of the I/V becomes more gradual than that of the ideal diode. The latter feature is often observed and referred to as low fill factor (FF).

C. Fluctuations

One verifiable prediction of the above picture is that the relative fluctuations of the main device parameters will diverge under low light, namely for D=2

$$\frac{\delta J_{sc}}{J_{sc}}, \frac{\delta V_{oc}}{V_{oc}}, \frac{\delta(FF)}{FF} \propto \begin{cases} I^{-1/2} & \text{for} \quad I < I_c, \\ const & \text{for} \quad I > I_c. \end{cases} \qquad (20)$$

To explain Eq. (20) we proceed from the fact that a point lateral nonuniformity causes the electric potential scaling as $V(r/L)$ with the coordinate r. The corresponding micro-current then becomes $\delta j \propto \nabla V \propto L^{-1}$. When $L/d \ll 1$, the current fluctuation felt by the probe is $\delta J \approx \delta j \sqrt{N} \propto L^{-1} L^{D/2} \propto I^{(D-2)/2}$, where $N \sim L^D$ is the number of shunts (weak diodes) in the active domain $\sim L^D$ (see Fig. 7). In the mean time, as is also seen from Fig. 7, the average short-circuit current, $J_{sc} \approx V_{oc}/\rho$ is logarithmic in intensity, simply following $V_{oc} \propto \ln J_{sc}$. As a result, the relative current fluctuation $\delta J_{sc}/J_{sc} \propto I^{(D-2)/2}$ is practically independent of the light intensity when $L/d \ll 1$ and D=2. In the low light regime, $L/d \gg 1$ the number of shunts N does not depend of L and is determined by the entire device area, while J_{sc} is proportional to the light intensity. Incorporating these changes yields $\delta J_{sc}/J_{sc} \propto 1/LI \propto 1/\sqrt{I}$. The crossover intensity I_c between the two regimes is determined by the condition $L = d$. (Note that in the 1D case the divergency $\sim I^{-1/2}$ holds both for $L \ll d$ and $L \gg d$.) It is straightforward to extend the above reasoning to the parameters V_{oc} and FF. Because $V_{oc} \propto \ln J_{sc}$, one gets $\delta V_{oc}/V_{oc} \propto \delta J_{sc}/(J_{sc} \ln J_{sc}) \sim \delta J_{sc}/J_{sc}$. The fill factor is sensitive to both the current and the potential (although the exact dependence is not known). In the first approximation one can write $\delta FF/FF \sim \delta J_{sc}/J_{sc} + \delta V_{oc}/V_{oc}$. Thus, the relative fluctuations in V_{oc} and FF depend on the light intensity similarly to that of J_{sc} and the FF relative fluctuation is roughly twice as large as the other two.

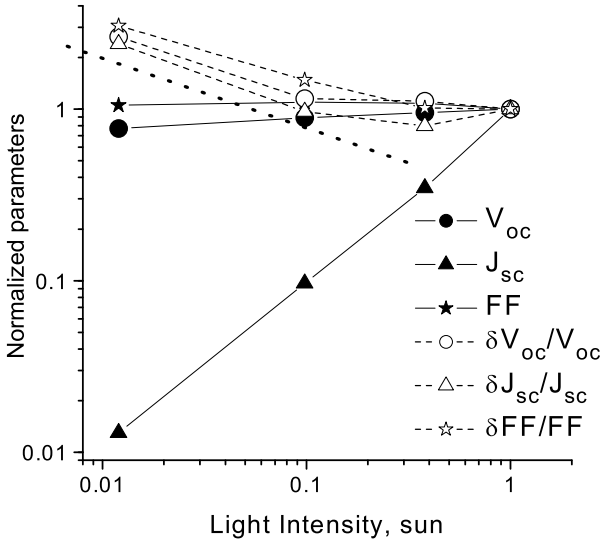

FIG. 8: The average PV parameters open-circuit voltage V_{oc}, short-circuit current J_{sc} and fill factor FF (solid symbols and lines), and their relative standard deviations (open symbols, dashed lines) versus light intensity normalized to the respective values at 1 sun and measured for an ensemble of 130 vapor transport deposited cells. Note the logarithmic scale: the standard deviations increase by a factor of 3 as the light intensity decreases by a factor of 10. The dotted line shows the predicted slope of the light intensity to the power -0.5.

To verify the prediction in Eq. (20) we studied fluctuations in the main PV parameters of 180 standard CdS/CdTe cells (efficiencies in the range of 10%) made by vapor-transfer deposition as described in Ref. 14. These cells are thin-film junctions sandwiched between two roundish (D=2) electrodes (area 1.1 cm^2), of which one is the TCO with sheet resistance $\rho = 15\Omega/\square$ and the other is a metal layer of negligibly small resistance. Our results in Fig. 8 are in excellent agreement with Eq. (20) (see also Ref. 45). Our estimate for the crossover intensity $I_c \sim 0.1$ sun is consistent with the observations when we take $L \sim L_0$ [consistent with Eq. 10)]. We have also verified that the relative fluctuations in FF are roughly twice as large as that in J_{sc} and V_{oc}.

D. Degradation

Another significant effect is nonuniform degradation,[18–20] caused by the electric current localization in a weak microdiode. This entails a corresponding increase in the carrier concentration, local surface charge, and Joule heat. The related degradation mechanisms are (i) electromigration of impurity ions; (ii) accelerated defect creation by excessive local carrier concentration; (iii) local electrochemical modification (corrosion, etc.) induced by ions from the ambient attracted to the excessive electric charges in the weak microdiode ends; (iv) direct action of locally increased

current or heat. All the above mechanisms will make the originally weak microdiodes degrade still more, thus increasing the degree of nonuniformity and accelerating the degradation: the laterally nonuniform system turns out to be unstable under light-induced or other bias.

Shown in Fig. 9 is an example of light-induced degradation where the cells were half-screened under the light soak at open circuit. After the soak, the screens were removed and the formerly screened (dark) and open (light) halves were electrically isolated from each other. The main observations are (i) the light and dark half degradations are comparable; (ii) the V_{oc} degradation is uniform so that light and dark halves degrade equally; (iii) the short-circuit current J_{sc} degrades nonuniformly so that either the light or the dark half deteriorates significantly but not both. Two conclusions can be made. First, it is not the light *per se*, but rather light-induced forward bias that causes the degradation (since there is little difference between the screened and open part degradation, and the screening length L is greater than the cell size). Second, the degradation does result in weak diodes (in either part of the cell) that rob significant current.[18] Both conclusions are consistent with the above-described picture of nonuniform degradation. We note that the philosophy of nonuniform degradation is not unique to the subject of this paper. Other examples, such as mechanical, electrical, and biological breakdowns, also show how nature concentrates stress on nonuniformities as different systems deteriorate. It is the more surprising then that the nonuniform degradation scenario has so far remained overlooked in photovoltaics and remains to be explored much more fully.

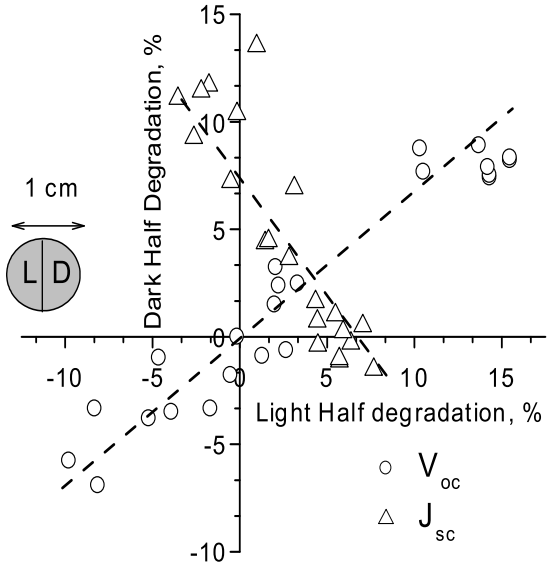

FIG. 9: Relative degradation of light and dark halves of half-screened cells under light soak. Each datum point corresponds to the two halves of one cell that had been half screened under the light soak. Dashed lines represent linear trends. Positive and negative values are chosen to represent the light-induced parameter decrease and increase, respectively. A gray circle sketches a cell broken into the light (L) and dark (D) halves.

Overall, we conclude that the effects of micrononuniformities are stronger under forward bias and/or low current conditions and result in current loss, low fill-factor behavior and fluctuations in device parameters. In addition, lateral micrononuniformities cause progressive nonuniform degradation. Furthermore, while being localized spatially they have a detrimental effect on the entire device.

V. TOWARDS QUANTITATIVE THEORY OF RANDOM DIODE ARRAYS

A problem of random diode arrays introduced in the present work, is a new nonlinear problem that properly belongs in the theory of disordered systems. Its quantitative analysis is quite involved and has not been fully developed. In fact, our semi-quantitative estimates in the preceding sections were aimed at partially substituting for such an analysis. In this section we describe one more rigorous approach to the problem.

The electric potential distribution in the diode circuit of Fig. 4 can be described more quantitatively based on the ideal diode equation (2) and the Ohm's law:

$$\nabla \mathbf{i} = -j_0 \left[\exp\left(\frac{e(V - V_{oc})}{kT} \right) - 1 \right], \qquad (21)$$

$$\rho \mathbf{i} = -\nabla V, \qquad (22)$$

where $\mathbf{i}$ is the lateral current (current density) in the resistive electrode for D=1 (D=2), V is the electric potential, and j_0 is the specific transversal currents (per length for D=1 or per area for D=2) defined in accordance with Eq. (2).

For the case of a point perturbation in the uniform system, Eqs. (22) reduce to the dimensionless form

$$\nabla^2 \phi = \exp(\phi) - 1, \qquad (23)$$

where

$$\phi = \frac{e(V - V_{oc})}{kT}, \quad y = \frac{x}{L_0}, \quad L_0 = \sqrt{\frac{kT}{e\rho j_0}}, \qquad (24)$$

and ∇ is calculated with respect to a new variable y. Note that Eq. (24) reintroduces in a more rigorous way the minimum screening length L_0. The solutions to Eq. (23) were analyzed for different types of point perturbations in Ref. 44.

For a nonuniform system we consider the case of strongly interacting diodes, $l \ll L$ and assume uncorrelated disorder. We use the dimensionless units of Eq. (24) where V_{oc} is replaced by $\overline{V}$ defined in Eq. (13). In

these units, the inequality $l \ll L$ becomes $l \ll 1$. It is convenient then to introduce a random variable

$$\zeta = \exp\left(-\frac{e(V_{oc} - \overline{V})}{kT}\right) - 1, \quad \langle\zeta\rangle = 0, \tag{25}$$

whose correlation function has the form

$$\langle\zeta(0)\zeta(\mathbf{r})\rangle = B\delta(\mathbf{r}), \quad B = const. \tag{26}$$

Here $\delta(\mathbf{r})$ is the delta-function of the coordinate $\mathbf{r}$ in the film plane. [Because of the micro-diode finite size, $\delta(\mathbf{r})$ should be understood as having a small yet finite width $l \ll 1$].

In place of Eq. (23), we now have

$$\nabla^2\phi = (1+\zeta)\exp(\phi) - 1, \tag{27}$$

Given the statistics for ζ Eq. (27) can be used to derive the distributions for the electric potential and current. From the perspective of the theory of disordered systems, Eq. (27) represent a new nonlinear problem. Our approach to its solution is somewhat similar to the well-known adiabatic approximation and utilizes the inequality $l \ll 1$. We present the electric potential as a superposition of the short-range (ϕ_s) and long-range (ϕ_L) components,

$$\phi = \phi_s + \phi_L, \quad |\phi_s| \ll 1, \quad \langle\phi_s\rangle = 0. \tag{28}$$

ϕ_s has the characteristic space scale $l \ll 1$. Its amplitude is assumed to be small, since the neighboring microdiodes separated by distance l and correspondingly small electrical resistance are at almost the same electric potential; the smallness condition is derived below [see Eq. (39)]. The long-range component is not necessarily small and is approximately constant on the scale of l.

Linearizing Eq. (27) in $|\phi_s| \ll 1$ and averaging over a region of linear dimension x such that $l \ll x \ll 1$ leads to the equation for the long-range component

$$\nabla^2\phi_L = (1 + \langle\phi_s\zeta\rangle_x)\exp(\phi_L) - 1. \tag{29}$$

In accordance with the central limit theorem, a random quantity $\langle\phi_s\zeta\rangle_x$ should obey the Gaussian statistics. Its fluctuations are relatively small, since the averaging is taken over a large number of microdiodes.

Eliminating the terms absorbed by Eq. (29) and neglecting ϕ_s in its right-hand-side, linearized Eq. (27) becomes

$$\nabla^2\phi_s = \zeta\exp(\phi_L), \tag{30}$$

where ϕ_L is considered constant. A system of coupled equations (29) and (30) describe the long-range and short-range components of the electric potential.

We start with finding the average $\langle\phi_s\zeta\rangle_x$ that appears in Eq. (29). This is achieved through the correlation function $\langle\zeta(0)\phi_s(r)\rangle$, which turns into $\langle\phi_s\zeta\rangle_x$ as the distance is set to the minimum length scale, $r = l$. To estimate $\langle\zeta(0)\phi_s(r)\rangle$ we multiply Eq. (30) by $\zeta(0)$ and then average. This leads to the Poisson equation

$$\nabla^2\langle\zeta(0)\phi_s\rangle_x = B\delta(\mathbf{r})\exp(\phi_L), \tag{31}$$

whose particular solution is

$$\langle\zeta(0)\phi_s\rangle_x = \exp(\phi_L)\begin{cases} B|r|/2 & \text{for} \quad D=1, \\ (B/2\pi)\ln r & \text{for} \quad D=2. \end{cases} \tag{32}$$

Constants that may appear in its general solution must be determined from the boundary conditions.

Because Eq. (30) is restricted to the region $r \ll 1$, the standard boundary condition is hard to impose. Offering an alternative is the observation that, in the absence of other characteristic lengths, the correlation between ζ and ϕ_s should decay over distances r approaching the correlation length L [$L = 1$ in the units of Eq. (24)]. We take the latter observation as a boundary condition. The required decay automatically follows from Eq. (32) for the case of D=2 where the logarithm decreases as $r \to L$. For D=1, a negative constant needs to be added to the solution in Eq. (32) to ensure the decay. [The latter analysis of $\langle\zeta(0)\phi_s\rangle$ can be easily verified for the case of a small disorder where Eq. (27) becomes linear in ϕ.]

Substituting into Eq. (32) $r = l$ and adding $-BL/2$ for the case of D=1, yields

$$\nabla^2\phi_L = -\frac{1}{4\xi}\left[\exp(\phi_L + \ln 2\xi) - 1\right]^2 + \frac{1}{4\xi} - 1, \tag{33}$$

with

$$\xi = \frac{B}{2}\cdot\begin{cases} 1 & \text{for} \quad D=1, \\ (1/\pi)\ln(1/l) & \text{for} \quad D=2. \end{cases} \tag{34}$$

We observe that, while aimed at describing random diode arrays, Eq. (33) does not contain random variables. As explained in what follows, the factors that account for the disorder are different for the cases of small and large ξ.

One immediate result of the above analysis is that there exists a critical disorder, $\xi_c = 1/4$, such that the electric potential and current distributions are qualitatively different for the cases of $\xi < \xi_c$ and $\xi > \xi_c$. In the case of subcritical disorder $\xi < \xi_c$ one can calculate the average potential in the system by setting the left-hand-side zero in Eq. (33),

$$\langle\phi\rangle = \ln\left(\frac{1-\sqrt{1-4\xi}}{2\xi}\right). \tag{35}$$

This solution fails when $\xi > 1/4$. Furthermore, analyzing the corrections $\delta\varphi_L \equiv \varphi - \langle\varphi\rangle$ by perturbation technique, it is straightforward to see from Eq. (33) that the characteristic length scale and amplitude of nonuniformities diverge as ξ approaches $\xi_c = 1/4$. Below we consider the cases of subcritical and supercritical disorder separately.

The parameter ξ is a figure of merit for the nonuniformity effects in the system under consideration. To

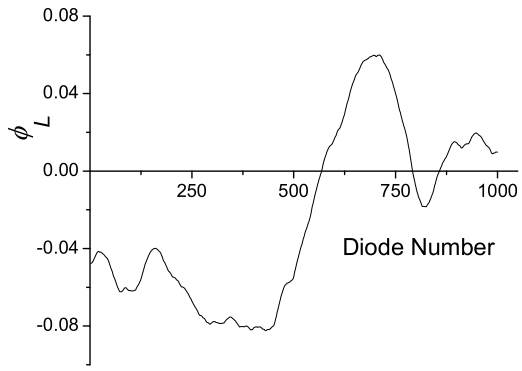

FIG. 10: 1D ϕ_L distribution for the case of subcritical disorder numerically simulated for a random diode circuit with uniformly distributed V_{oc}. The diode number plays the role of the linear coordinate. The distribution is characterized by the average $\langle eV_{oc}/kT\rangle = 10$ and the corresponding standard deviation 2. Note the scale of fluctuations, $|\delta\phi_L| \ll 1$.

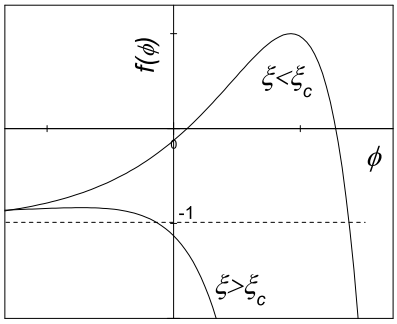

FIG. 11: Right-hand-side $f(\phi)$ of Eq. (33) for the cases of subcritical ($\xi = 1/8$) and supercritical ($\xi = 3/2$) disorder. Note that $f(\phi) < 0$ in the latter case.

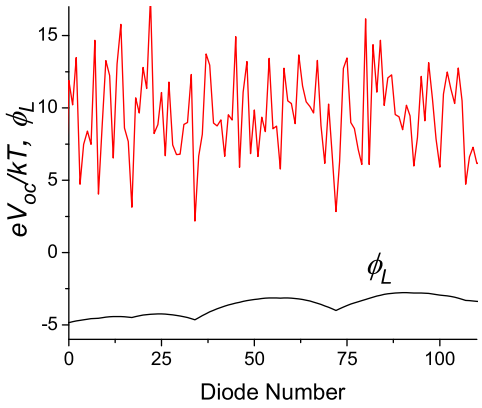

FIG. 12: A fragment of V_{oc} and reduced electric potential ϕ distributions for the case of supercritical Gaussian disorder numerically simulated for a 1D random diode circuit. Note singular ϕ shapes in the proximity of minima, which coincide with the lowest V_{oc}s, and parabolic coordinate dependence of almost the same curvature far from the minima.

explain its physical meaning we consider the case of bimodal V_{oc} distribution where weak diodes are found with a probability $c(\ll 1)$. The coefficient B in Eq. (26) can be then estimated (in conventional units) as

$$B \sim c\left(\frac{l}{L}\right)^D \exp\left[2\frac{e(\overline{V}-V_{oc})}{kT}\right]. \qquad (36)$$

Taking into account also the estimate $c \sim l/R$, it is straightforward to see that $\xi \approx \xi_R$ where the average distance between the weak diodes R and the disorder parameter ξ_R were discussed in Sec. III [see Eq. (11)]. Hence, ξ represents the relative dispersion of the weak diode bare currents.

Subcritical disorder. The required average $\langle\zeta(0)\phi_s\rangle_x$ was calculated in the above through the correlation function $\langle\zeta(0)\zeta(\mathbf{r})\rangle$ defined for the infinite system in Eq. (26). As was discussed after Eq. (29), the finite size effects will make B a Gaussian random quantity with the relative standard deviation of the order of $(l/x)^{D/2} \sim l^{D/2} \ll 1$. For small $\xi \ll 1$ the right-hand-side in Eq. (33) $f(\phi)$ is dominated by the contribution that is inversely proportional to ξ and the variations $\delta\xi$ become important source of randomness. Because the latter are small, so are the variations in ϕ. They satisfy the linearized equation (33) that is

$$\nabla^2\delta\phi_L = \langle\phi\rangle\sqrt{1-4\xi}\,\delta\phi_L - \delta\xi\exp\langle\,2\phi\rangle. \qquad (37)$$

We conclude that fluctuations $\delta\phi$ obey Gaussian statistics and are small in the measure of $\delta\xi$. As an illustration, shown in Fig. 10 is a distribution $\delta\phi(x)$ numerically simulated for a system of random diodes with subcritical disorder. It has a smoothly varying shape similar to what is typically considered random potential in the existing theory of disordered systems (see for example Ref. 48).

Supercritical disorder. To understand the case of $\xi > \xi_c$ we note that the right-hand-side of Eq. (33), $f(\phi)$ (and thus the curvature $\nabla^2\phi$) is everywhere negative as illustrated in Fig. 11. The negative curvature exponentially increases in absolute values as ϕ increases above its maximum $\phi_m = \ln(1/2\xi)$. This means that the spectrum of ϕ cannot span much beyond ϕ_m, since any increase in ϕ (i. e. positive $\nabla\phi$) is strongly limited by exponentially large negative $\nabla^2\phi$.

For large $\xi \gg \xi_c$ and $\phi < \phi_m$ we find $f(\phi) \approx -1$. Therefore, $\phi(\mathbf{r})$ is close to a negative curvature paraboloid and is unbounded below. This is consistent with the above observation that the average $\langle\varphi\rangle$ is not defined for the case of $\xi > \xi_c$. The unbounded spectrum exists in the framework of the approximation employed.

We now consider lower boundary effects beyond that

approximation. The lowest ϕ in the system corresponds to the weakest diode. In the framework of our approximation, it exhibits a singularity where $\nabla\phi$ undergoes a finite change and the electric potential cannot be decomposed into a sum of long- and short-range components. Taking such singularities into account, we conclude that the electric potential has a piecewise continuous structure. It is formed by a set of negative curvature paraboloids (far from weak diodes where the approximation of smoothly varying potential is valid), connected in a singular way at weak diodes. The singularities take place at the diodes that are the weakest in the neighborhood of screening length size each. This understanding has been confirmed by our numerical simulations for both the cases of 1D (Fig. 12) and 2D (Fig. 13) random diode circuits, which show, indeed, randomly located negative curvature paraboloids forming cusps in connection points. Note that for the case of supercritical disorder the electric potential spatial nonuniformity is mainly due to random spatial distribution of weak diodes.

If the V_{oc} distribution is not a bimodal, then the location of singularities needs to be further specified. A diode weakest in its screening length neighborhood ($V_{oc} = V_{oc,\min}$) will obviously cause a singularity. On physical grounds, a less weak diode at distance r in the neighborhood will cause a singularity if its V_{oc} is less than $V_{oc,\min} + j_0\rho r^2$ to make it a local current sink. While consistent with the results of numerical modelling this remains a plausible assumption.

Note that the piecewise continuous type of disorder revealed in the above study is rather unusual from the perspective of the existing theory of disordered systems.[48] This unique feature adequately reflects the fact that random microdiodes in the array are exponentially different. The weakest of them dominate the electric potential distribution in the system and make all more robust units immaterial.

As an example consider one implication of the above theory, which is the statistics of stronger-than-average "shunting" currents in a system of random microdiodes. The probability of finding no weak diode in the region of large radius $r > R$ is given by the Poisson distribution $\exp[-(r/R)^D]$, where R is the average distance between weak diodes. Because the amplitude of electric potential $\delta\phi$ is parabolic in r, we get $\delta\phi \propto r^2$. The electric current can be expressed as $J \sim \delta\phi/(\rho r^{(2-D)})$ where $D = 1, 2$ [see the discussion after Eq. (3)]. As a result the probability distribution for the current takes the form

$$g(J) \propto \exp(-J/J_0) \quad \text{for} \quad J > J_0, \tag{38}$$

for both the cases of D=1 and D=2 where $J_0 = j_0 R^D = const$. This prediction is verified by numerical simulations in Fig. 14: good agreement is obtained.

The above-developed approximation is based on linearization of Eq. (27) with respect to ϕ_s, and remains valid when $\langle\phi_s^2\rangle \ll 1$. Multiplying Eq. (30) by $\phi_s(0)$, averaging, and taking into account Eqs. (32) and (34),

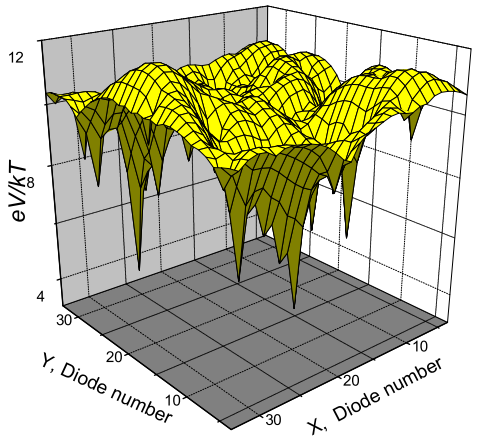

FIG. 13: Reduced electric potential ϕ distribution for the case of 2D supercritical disorder numerically simulated for a random diode circuit of 31x31 diodes. Note piecewise continuous topography with cusp shapes in the proximity of minima and paraboloidal coordinate dependence far from the minima.

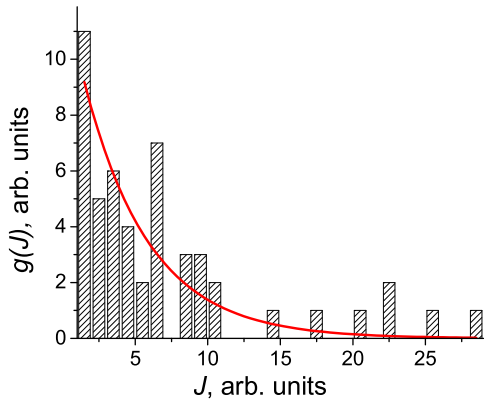

FIG. 14: Distribution of weak diode electric currents in a system of random diodes with supercritical disorder: numerical simulations (histogram) vs. analytical fit of Eq. (38).

yields

$$\langle\phi_s^2\rangle = \xi \exp(2\phi_L). \tag{39}$$

The criterion $\langle\phi_s^2\rangle \ll 1$ is obviously satisfied for the case of subcritical disorder $\xi \ll 1$. For the alternative case of $\xi \gg 1$ we take into account that the spectrum of ϕ_L is confined to the region $\phi_L \lesssim \ln(1/2\xi)$. As substituted in Eq. (39) this gives $\langle\phi_s^2\rangle \lesssim 1/4\xi$, which satisfies the criterion $\langle\phi_s^2\rangle \ll 1$ in the far supercritical region $\xi \gg \xi_c = 1/4$. Our approximation fails in the critical region $\xi \sim \xi_c$.

We shall end this section by noting that the above approximation, while giving a consistent picture of the elec-

tric potential distribution in a system of random diodes, leaves many important questions unanswered. Those of the statistics of random electric potential and currents, the boundary conditions for finite systems, and integral I-V characteristics seem to be the most appealing ones. We hope to address these issues elsewhere.

VI. BLOCKING THE EFFECTS OF NONUNIFORMITIES

As a semiconductor thin-film device is deposited, not much can be done to improve its disordered structure. The known remedies are chemical treatments (such as $CdCl_2$ for CdTe photovoltaics) and anneals, which increase and equalize grain sizes and otherwise promote uniformity. Here we would like to point toward other remedies, which, while keeping the semiconductor structure intact, can significantly reduce the device nonuniformity. As is seen from Fig. 4, the steeper the I/V curve in the forward bias region $V > V_{oc}$, the stronger the impact of a weak diode. (In particular, the exponential bias dependence in Eq. (2) led to the exponentially strong weak diode effects as discussed above.) The exponential steepness is known to reduce to a linear bias dependence when there is a considerable series resistance added to the elemental diode. Hence, increasing the series resistance will mitigate the detrimental effects on micrononuniformities. We verified the latter argument by numerically simulating the circuit in Fig. 4 with series resistances added to each of the random diodes: a significant suppression of the electric current and electric potential lateral fluctuations was indeed observed.

The above prediction of the beneficial role of series resistance has two practical implications. First, the general quest for decreasing the device series resistance may not be justified in all cases. While this minimizes the ohmic loss, it can simultaneously promote losses due to micrononuniformity effects. The analysis above shows that the series resistance should be carefully optimized to compromise between the ohmic and the micrononuniformity-related losses. Such optimization should open opportunities in thin-film device engineering.

The second implication has to do with buffer-layer effects,[49] which, while proven generally positive, remain poorly understood. We recall that the buffer layer is generally a resistive, thin layer placed between the semiconductor and TCO. Because of its small thickness, it does not add much to the device series resistance. In the mean time it is known to minimize current losses in the device and in some cases to improve the device stability. From the perspective of this paper, a beneficial effect of the buffer layer is that it adds series resistances to the weak diodes (or shunts). In understanding this effect it is crucial to take into account the characteristic micrononuniformity size l. The series resistance of the "clog" added by the buffer layer to a weak diode or shunt, $r_{bl} \propto l^{-2}$ is significant for small size micrononuniformities, but may have no effect on nonuniformities of considerable lateral dimensions. Hence, the same buffer layer may or may not have positive impact on the device performance and stability, depending on details of the device technology affecting the micrononuniformity length scale. We believe that the buffer layer should be optimized based on the device uniformity characteristics.

Finally, we note that the above-discussed physics not only explains how nonuniformities are detrimental to device performance and stability, but also suggests a certain way of levelling them out. Namely, because the surface potential (local V_{oc}) under the light varies across a semiconductor film, electrochemical treatments sensitive to the electric potential will act differently at different spots. When properly chosen they should deposit clogs onto the weak diode spots while leaving the robust parts of the film practically intact, thus eliminating the most significant sources of nonuniformity effects. It is likely that in such treatments have already been found in several cases by trial and error. In particular, that might explain why different pre-contact treatments, including weak etches and exposure to organics have a profound effect on device parameters. We believe that our present consideration provides the understanding to search effectively for the desired treatments. In our most recent work[50] we have verified the above prediction of the electrolyte treatment effect: $\sim 50\%$ increase in the device efficiency was found.

VII. CONCLUSIONS

In conclusion, we have shown that large-area semiconductor devices are intrinsically nonuniform, which makes their physics qualitatively different from that of microelectronics. The nonuniformity length scales cover a broad spectrum ranging from microns to meters. They show up in many different types of experiments and for the majority of thin-film semiconductors. We have also found a characteristic screening length that ranges from millimeters to meters and explains how a microscopic nonuniformity can affect macroscopically large areas in the film. Our theoretical model (of random diodes) explained some of the observed features. We described the electric current and potential fluctuations and their effect on the main parameters of thin-film devices. Our consideration here has suggested certain ways of overcoming these nonuniformity effects.

Our present consideration was mostly restricted to an elemental PV cell. Another closely related application should be mentioned where the concepts of nonuniformity and random diode arrays can be extremely important, which is the macroscopic circuitry of large area PV modules and their field arrays. A typical PV module is composed of a large number (~ 100) linear cells *in series*. Because of the cell diode nature, these series will be very sensitive to small variations in the cell parameters;

hence, the problem of random diodes in series. Furthermore, in the field, photovoltaic arrays form more complex circuits where, for example, blocks of many modules in parallel are connected in series. Again, since the modules have slightly different characteristics,[2,51] the latter systems will belong to the class of random diode systems. A relevant theoretical approach is needed to understand their physics and optimize the design.

We hope this work will facilitate more systematic study of nonuniformities in large area electronics. We believe that enhanced understanding of the nonuniformity effects will help to improve thin-film device performance and stability in many applications. We hope also that a new class of disordered systems that is the random diode arrays presented in this work will attract more attention to become a practically important challenging problem in the physics of disordered systems.

Acknowledgment

This work was partially supported by the NREL grant nos. ZAF-8-17619-14 and NDJ-1-30630-02. The authors would like to thank First Solar, LLC, for some of the cell structures used in this study. We are also grateful to G. Dorer, V. Kaydanov, B. von Roedern, and K. Zweibel for invaluable discussions.

---

* Electronic address: vkarpov@physics.utoledo.edu

[1] S. M. Sze, *Physics of Semiconductor Devices* (Willey & Sons, New York, 1981).

[2] H. S. Ullal, K. Zweibel, and B. G. von Roedren, *Proc.* 28 *th IEEE Photovoltaic Specialists Conference*, Alaska, p. 418 (2000).

[3] D. Eich, U. Hereber, U. Groh, U. Stahl, C. Heske, M. Marsi, M. Kiskinova, W. Reidl, R. Fink, E. Umbach, *Thin Solid Films*, Vol. 361-362, 258 (2000).

[4] G. A. Medvedkin, L. Stolt, and J. Wennerberg, *Semiconductors* **33**, 1037 (1999).

[5] J. Ermer, R. Gay, D. Pier and D. Tarrant, *J. Vac. Sci. Technol.* **A11**, 1888 (1993).

[6] Jin-Hui Tan, W.A. Anderson, *Solar Energy Mater. Solar Cells*, **77**, 283 (2003).

[7] S. A. Galloway, A. W. Brinkman, K. Durose, P. R. Wilshaw and A. J. Holland, *Appl. Phys. Lett.* **68**, 3725 (1996).

[8] P. R Edwards, S. A. Galloway and K. Durose, *Thin Solid Films* **372**, 284 (2000).

[9] R. Harju, V. G. Karpov, D. Grecu and G. Dorer, *J. Appl. Phys.* **88**, 1794 (2000).

[10] T. J. McMahon and B. G. von Roedern, *Proc. 26th IEEE Photovoltaic Specialists Conference*, Anaheim, CA, 375 (1997).

[11] I. L. Eisgruber, R. J. Matson, J. R Sites and Emery, K. A. , *Proc. 1st World Conference on Photovoltaic energy Conversion*, 283, Hawaii (1994).

[12] P. N. Gibson, M. A. Baker, E. D. Dunlop, M. E. Ozsan, D. Lincot, M. Froment, G. Agostinelli, *Thin Solid Films* **387**, 92 (2001).

[13] R. K. Ahrenkiel, B. M. Keyes, D. L. Levi, K. Emery, T. L. Chu, and S. S. Chu, *Appl. Phys. Lett.*, **64**, 2879 (1994).

[14] D. Shvydka, A. D.Compaan, and V. G. Karpov, *J. Appl. Phys.* **91**, 9059 (2002).

[15] I. M. Dharmadasa, C. J. Blomfield, C. G. Scott, R. Coratger, F. Ajustron, and J. Beauvillain, *Solid State Electronics*, **42**,. 595 (1998).

[16] C. F. Alonso,M. P. Hernandez, E. Cassielles, and J. L. Pena, *Appl. Phys. Lett.*, **80**, 3751 (2002).

[17] D. Shvydka, A. D. Compaan, and V. G. Karpov, unpublished.

[18] V. G. Karpov, R.Harju and G. Dorer, *Proc. 28th IEEE Photovoltaic Specialists Conference*, Alaska, 547 (2000).

[19] V. G. Karpov, A. D. Compaan and D. Shvydka, *Appl. Phys. Lett.* **80**, 4256 (2002).

[20] A. O. Pudov, M. Gloeckler, S. H. Demtsu, and J. R. Sites, K.L. Barth, R.A. Enzenroth, and W.S. Sampath, *Proc.* 29 *th IEEE Photovoltaic Specialists Conference*, New Orlean, 760 (2002).

[21] D. Rose, R. Powell, U. Jayamaha, M. Maltby, *Proc.* 29 *th IEEE Photovoltaic Specialists Conference*, New Orlean, 555 (2002).

[22] N. Sakikawa, M. Tamao, S. Mayazaki, and M. Hirose, *Jpn. J. Appl. Phys.* **38,** 5768 (1999).

[23] U. K. Das, J. K. Rath, D. L. Williamson and P. Chaudhuri, *Jpn. J. Appl. Phys.* **39**, 2530 (2000).

[24] R. Baldner, H. Lautenschlager, C. Schetter, R. Schindler, W. and Warta, 25 *th IEEE Photovoltaic Specialists Conference*, Washington DC, 641 (1996).

[25] I. Tarasov, S. Ostapenko and J. P. Kalejs, *Proc. 28th IEEE Photovoltaic Specialists Conference*, Alaska, 112 (2000).

[26] B. Rezek, C. E.Nebel and M. Stutzmann, *Appl. Phys. Lett.* **75**, 1742 (1999).

[27] J. P. Boyeaux, A. Kaminski, N. Ferrer, S. Berger & A. Laugier, *Proc. 28th IEEE Photovoltaic Specialists Conference*, Alaska, 319 (2000).

[28] A. S. H. van der Heide, A. Schonecker, G. P. Wyers, and W. C. Sinke, *Proc. 16th European Photovoltaic Solar Energy Conference, Glasgow*, p. 419 (2000).

[29] K. Kurobe, M. Miura, K. Hirano, H. Matsunami, *Solar Energy Mater. Solar Cells*, **74**, 183 (2002).

[30] J. Carstensen, G. Popkirov, J. Bahr, H. Foll, *Solar Energy Mater. Solar Cells*, **76**, 599 (2003).

[31] O. Breitenstein, K. Iwig, K. and I. Konovalov, *Phys. Stat. Sol. (a)* **160**, 271 (1997).

[32] I. Konovalov, O. Breitenstein and K. Iwig, *Solar Energy Materials and Solar Cells* **48**, 53 (1998).

[33] O. Breitenstein and M. Langenkamp, *Proc. 2nd World Conference on Photovoltaic Solar Energy Conversion*, Vienna, Austria, 1382 (1998).

[34] Kh. G. Naghmudinov and T. A. Polyanskaya, *Sov. Phys. Semicond.* **21**, 1053 (1987).

[35] L. E. Calvet, R. G. Wheeler, and M. A. Reed, *Appl. Phys. Lett.* **80**, 1761 (2002)

[36] W. Monch,*J. Vac. Sci. Technol. B* **17**, 1867 (1999).

[37] B. A. Morgan, K. M. Ring, K. L. Kavanagh, A. A. Talin, R. S. Williams, T. Yasuda, T. Yasui, Y. Segawa, *J. Vac. Sci. Technol.* B **14**, 1238 (1996).

[38] H. J. Im, Y. Ding, Y., J. P. Pelz and W. J. Choyke, *Phys. Rev. B* **64**, 075310-1 (2001).
[39] R. T. Tung,*Appl. Phys. Lett.* **58**, 2821 (1992).
[40] M. E. Raikh and I. M. Ruzin, in *Mesoscopic Phenomena in Solids*, (eds Altshuller, B. L., Lee, P. A. and Webb, R. A.) 315 (Elsevier, 1991).
[41] R. Tenne, V.Marcu and N. Yellin *Appl. Phys. Lett.* **45**, 1219 (1984).
[42] F. Roccaforte, F. Via, V. Raineri, R. Pierobon, and E. Zanoni, *J. Appl. Phys.* **93**, 9137 (2003).
[43] M. Amman, J. C. Lee, and P. N. Luke, *J. Appl. Phys.* **92**, 3198 (2002).
[44] V. G. Karpov, G. Rich, A. V. Subashiev and G. Dorer, *J. Appl. Phys.* **89**, 4975 (2001).
[45] D. Shvydka, A. D. Compaan, and V. G. Karpov, Appl. Phys. Lett., **82**, 2157 (2003).
[46] G. Lucovsky, J. Appl. Phys. **31**, 1088 (1960).
[47] The fact that L depends on u, makes the definition in Eq. (7) implicit. To the logarithmic accuracy, L in the right-hand-side of Eq. (7) can be replaced by its minimum value L_0.
[48] I. M. Lifshits, S. A. Gredeskul, and L. A. Pastur, *Introduction to the Theory of Disordered Systems*, John Wiley, New York 1988.
[49] Bolko von Roedern, *Mat. Res. Soc. Symp. Proc.* **668**, H6.9.1 (2001)
[50] V. G. Karpov, D. Shvydka, Y. Roussillon and A. D. Compaan, in *Proc. of 3rd World Conference on Photovoltaic Energy Conversion*, Osaka, Japan, May 2003, in press.
[51] K. Kushiya, M. Ohshita, I. Hara, Y. Tanaka, B. Sang, Y. Nagoya, M. Tachiyuki, O. Yamase, *Solar Energy Mater. Solar Cells* **75**, 171, (2003)